CHEMISTRY OF MATERIALS

Article

pubs.acs.org/cm

Rapid Sol–Gel Fabrication of High-Quality Thin-Film Stacks on Planar and Curved Substrates

Moussa Barhoum, Jacob M. Morrill, David Riassetto, and Michael H. Bartl*

Department of Chemistry, University of Utah, 315 South 1400 East, Salt Lake City, Utah 84112, United States

Supporting Information

ABSTRACT: A versatile and rapid sol–gel technique for the fabrication of high quality one-dimensional photonic bandgap materials was developed. Silica/titania multilayer materials are fabricated by a sol–gel chemistry route combined with dip-coating onto planar or curved substrates. A shock-cooling step immediately following the thin-film heat-treatment process is introduced. This step was found crucial in the prevention of film crack formation—especially in silica/titania alternating stack materials with a high number of layers. The versatility of this sol–gel method is demonstrated by the fabrication of various Bragg stack-type materials with fine-tuned optical properties by tailoring the number and sequence of alternating layers, the film thickness and the effective refractive index of the deposited thin films. Measured optical properties show good agreement with theoretical simulations, confirming the high quality of these sol–gel fabricated optical materials.

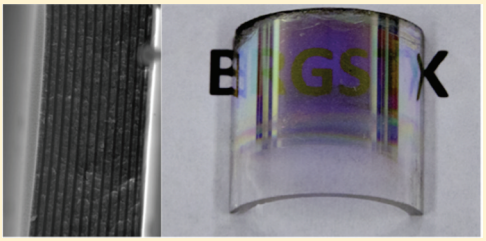

KEYWORDS: *sol–gel chemistry, dip-coating, thin-film, Bragg stack, Fabry–Perot microcavity, optical reflection spectroscopy*

INTRODUCTION

Sol–gel chemistry has emerged as an attractive—simple, rapid and inexpensive—alternative synthesis route to physical and chemical deposition methods.[1−6] The relatively mild synthesis conditions and flexibility of sol–gel chemistry have opened the door to a large variety of compounds that can be processed into thin films, fibers, and monoliths. In addition, when combined with molecular and/or colloidal assembly methods, it is possible to create composites with internal three-dimensional meso-to-macroscale periodic features and other hierarchical structures.[4−12] This large diversity of accessible compositions, morphologies and internal structures makes sol–gel chemistry-derived materials attractive candidates for numerous applications ranging from catalysis, separation, and sorption to uses in electronics and photonics.[4−6,13−18]

A remaining challenge for widespread commercial applications is to produce sol–gel-derived materials with structural uniformity over large sample areas (>cm^2) and controlled batch-to-batch reproducibility. This is particularly true for thin-film based materials and applications. Here, the level of uniformity and control over thin-film parameters has been set very high by physical and chemical deposition methods, such as atomic layer deposition,[19,20] chemical vapor deposition,[21,22] molecular beam epitaxy,[23] and various sputtering techniques.[24−26] Therefore, for sol–gel processing to be considered a viable fabrication alternative for commercial applications, similar standards have to be achieved. The two foremost challenges in sol–gel fabrication of thin films are the avoidance of crack formation and the achievement of a uniform and reproducible film thickness over large areas. Both of these problems are directly related to solvent evaporation during deposition of thin films (dip or spin coating, casting) and their densification in subsequent heat treatments (calcination, annealing).[5,27,28] Conducting the thin film deposition process under controlled environmental conditions (for example, a dedicated clean room with controlled humidity, temperature, substrate pretreatment, absence of dust particles in air) can help to significantly increase the film quality. However, despite these advances, sol–gel-derived thin films are still prone to irregularities in film thickness (edge effects), and shrinkage and crack formation during heat treatment.

Among the large family of interesting thin film compounds the wide bandgap semiconductor titania has recently gained tremendous attention due to its outstanding chemical and physical properties. While high chemical stability and catalytic activity make titania a prime candidate for photoanodes in solar cells[29] and water-splitting,[30,31] its high refractive index combined with optical transparency in the visible range of the electromagnetic spectrum are ideal for producing reflective coatings[32] and other optical components.[33] Furthermore, by depositing titania thin films alternatingly in stack form with a lower refractive index compound such as silica, interesting one-dimensional (1D) photonic bandgap materials can be fabricated, including reflectors, filters, and microcavities.[34−36] Such layering of thin films of different compounds with different thermal expansion coefficients, however, poses a big challenge for sol–gel fabrication. During film processing and thermal treatments, different shrinkage properties within alternating layers and at interfaces induces stresses and can

Received: July 14, 2011
Revised: October 27, 2011
Published: October 28, 2011

   dx.doi.org/10.1021/cm202019b | *Chem. Mater.* 2011, 23, 5177–5184

lead to severe crack formation, delamination, and variation in the film thicknesses.

A strategy for minimizing crack formation in titania/silica thin-film stacks is the firing process.[28,37] This is an additional short heat-treatment step at high temperatures (900−1000 °C). The purpose of this firing process is to take advantage of the opposing thin film stresses for silica and titania at 900 °C. While, studies by Rabaste et al.[37] and Kozuka et al.[28] revealed an induced tensile stress for both silica and titania thin films up to 800 °C, increasing the temperature to 900 °C resulted in a compressive stress for silica. It is argued that these opposing stresses result in an overall relaxed multistack and reduces the formation of cracks. Contrasting this high-temperature approach, Keszler et al. reported a low-temperature (5 °C) solution-processing method followed by an annealing step at modest temperatures (300 °C).[38] This method allows for the deposition of dense titania thin films. However, in this method the deposition thickness is limited to ∼18 nm for each deposition cycle. To create alternating stack structures with each layer having a thickness of several tens to hundreds of nanometer thickness (as required for application as photonic bandgap materials operating in the visible or near-infrared range), this method would require deposition of multiple consecutive films of the same compound.

In this paper, we describe an alternative sol−gel approach for the rapid fabrication of high quality silica and titania thin films and alternating silica/titania stack structures. Our method allows deposition of these thin films and multilayer structures on planar and curved structures without loss of film quality. Regardless of stack structure, layer numbers and type of substrate, the materials fabricated by our method have predictable uniform thickness and are crack-free over large areas. The versatility of our sol−gel method is demonstrated by engineering different 1D photonic bandgap materials on planar and curved substrates, including high quality Bragg reflectors and filters, Fabry−Perot microcavities, and asymmetric stacks. We show that the photonic properties of these structures can be readily tuned by controlling the thickness and sequence of the deposited films as well as by tailoring the refractive indices of individual layers through the introduction of nanoporosity. We will discuss the essential steps of our sol−gel deposition and processing method and introduce several new process parameters found to be critical for successfully producing crack-free multilayer structures with uniform thickness. These parameters include controlled solvent evaporation during and after the film deposition and a shock-cooling step immediately following the thermal annealing process at 350−500 °C. The fabrication steps and the final samples were characterized by scanning electron microscopy (SEM), transmission electron microscopy (TEM), variable-angle ellipsometry measurements, X-ray diffraction (XRD), and optical reflection spectroscopy. The measured optical reflection spectra are further compared to simulated spectra using the transfer-matrix method.[39]

EXPERIMENTAL SECTION

Preparation of Precursor Solutions. The titania precursor solution was prepared by mixing 60 mL of titanium(IV)isopropoxide (98%, Acros) and 65 mL of ethanol under vigorous stirring for 30 min (exothermic reaction). A solution of 124 mL of ethanol, 0.6 mL of hydrochloric acid (12 M) and 1.15 mL of 18 Ω deionized water (DI water) was then added to the titania solution and stirred for an additional 30 min. This titania precursor solution (titania stock solution) with a molar ratio of 1:16.15:0.42:0.097 titanium(IV)-isopropoxide:EtOH:H_2O:HCl was aged for at least 48 h at room temperature before further use. The silica precursor solution was prepared by adding 105 mL tetraethylorthosilicate (Aldrich) to a mixture of 12.3 mL of DI water, 76 mL of ethanol, and 6.3 mL of HCl (0.01 M) and mixing for 30 min at room temperature. This silica precursor solution (silica stock solution) with a molar ratio of 1:2.77:1.92:0.004 tetraethylorthosilicate:EtOH:H_2O:HCl was aged for at least 48 h at 60 °C before further use. Both the titania and the silica precursor solutions are stable for at least one week when stored in the dark.

Deposition of Thin-Film Single and Multilayer Structures. Figure 1 illustrates the four-step thin-film deposition cycle. Thin films

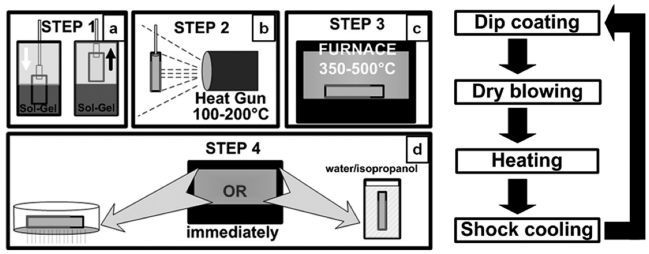

Figure 1. (Left) Thin-film deposition cycle for the fabrication of sol−gel thin-film layers. (a) Step 1, dip-coating; (b) step 2, dry-blowing; (c) step 3, heat-treatment (annealing); (d) step 4, shock-cooling. (Right) Flowchart depicting the main steps of the deposition cycle.

were deposited by dip-coating precursor solutions onto cleaned substrates. Cleaning was done by rinsing with isopropanol and drying in a stream of nitrogen. Substrates were immersed into the sol (titania or silica precursor solution) and vertically withdrawn at a constant speed of 12.5 cm/min (step 1). The dip-coating process was immediately followed by heating the deposited film in a flowing stream of hot air (100−200 °C; produced by a heat gun) for rapid evaporation of volatile solvents (step 2). The dried films were further heat-treated (calcined) for 1 min at 350−500 °C in a muffle furnace (step 3). The final step of the thin-film deposition cycle was a shock-cooling procedure (step 4). This was accomplished by taking the sample out of the hot furnace and either placing it onto a Pyrex glass substrate at room temperature or dipping it into a water/isopropanol mixture. The selection of the cooling method depends on the geometry of the substrate and the heat transfer ratio between the substrate and the heat sink. While the former method was sufficient to promote rapid cooling for thin films deposited onto thin silicon wafer substrates, the latter method was necessary for curved substrates and substrates made of thick silicon wafers and quartz or glass slides. Titania or silica single-compound multilayers and alternating titania/silica multilayer stacks were prepared by repeating this cycle using the appropriate sols at each cycle. A final heat-treatment of the multilayer structures at 400−500 °C for 1 h concluded the deposition process.

Fabrication of Bragg Stacks and Fabry−Perot Microcavities. Bragg stacks (reflectors, filters) were fabricated by deposition of at least 6 alternating silica/titania double-layers (12 layers in total). The thickness of each layer was controlled by either diluting the precursor solutions with additional ethanol or by varying the dip-coating speed, allowing for tuning the optical bandgap in the visible range as discussed further in the Results and Discussion section. For example, to fabricate a silica layer with a thickness of 88 ± 2 nm the original silica stock solution was diluted down to 25 vol % of its original value. The fabrication of 80 ± 2 nm titania layer requires a 20 vol % dilution of the stock solution with ethanol. This relationship of film thickness and degree of dilution of the precursor solutions is also depicted in Figure S1 (Supporting Information). Fabry−Perot optical microcavities were fabricated by breaking the symmetry of a Bragg stack, i.e., introduction of a "defect layer". This was accomplished by subsequently depositing two layers of the same compound. The wavelength position and quality of the microcavity mode was tuned by adjusting the thickness and dielectric properties of the defect layer with respect to the multilayer stack.

dx.doi.org/10.1021/cm202019b | Chem. Mater. 2011, 23, 5177−5184

Refractive Index Tuning. The films' effective refractive index was tuned by introducing a certain degree of nanoporosity into a deposited dielectric layer. This was achieved by dissolving various amounts of the block copolymer surfactant Pluronic P123 in the sol prior to dip-coating.[6,40] For example, to lower the refractive index of a titania layer, between 0.1 and 0.5 g of P123 were dissolved in the titania precursor solution (described above). To compensate for changes of the solution viscosity due to the addition of surfactants, the dip-coating speed was adjusted to keep the thickness of the deposited layers constant. Heat-treatment of the samples caused the pyrolitic removal of the surfactant molecules and formation of a disordered nanoporous framework. This framework was then infiltrated during the succeeding deposition cycle by the alternating precursor solution (e.g., silica), resulting in a lowered effective refractive index from pure titania to that of a titania/silica composite.

Characterization Studies. The film crystallinity was determined by a Bruker D8 Advanced X-ray Diffractometer (Cu−Kα radiation). The refractive index and thickness of thin films were measured with a Woolam Variable Angle Spectroscopic Ellipsometer. SEM studies were conducted on a FEI NovaNano (FEG-SEM630) microscope and a FEI NovaNano (FEI DB237) focused ion beam microscope. TEM imaging was done on a FEI Tecnai F30 microscope at 300 kV acceleration voltage. Sample preparation for TEM measurements involved scratching off the deposited thin film from the Si-waver substrate with a sharp razor blade. The sample was then suspended in ethanol and dispersed onto a copper TEM sample holder. Sample preparation for SEM measurements involved splitting the thin film substrate perpendicular to the deposited thin film stack and mounting the exposed cross section of the sample on a vertical SEM specimen stub. If necessary the mounted specimen was coated with a thin layer of gold to minimize charging effects during SEM studies.

Optical Reflection Microscopy and Spectroscopy. Optical reflection spectra were measured with a modified optical microscope (Nikon ME600). The output of a broadband white light source was focused onto the sample surface by a 20× objective (0.45 NA). The reflected light was collected by the same objective and either imaged by a CCD camera or fiber-coupled into an Ocean Optics USB-4000 UV−vis spectrometer. A broadband mirror ($R > 0.96$) was used as reference.

Simulation of Optical Reflection Spectra. Optical reflection spectra were simulated by the transfer-matrix method using OpenFilters.[41] OpenFilters is an open-source software with a built-in graphical interface and is available at no charge under the GNU General Public License.

RESULTS AND DISCUSSION

Single and Multilayer Sol−Gel Dip-Coating Process.

The dominating challenge in fabricating high-quality thin film single and multilayer structures is the suppression of crack formation. Crack formation is the result of stresses occurring during and after the deposition process that exceed the thin film strength.[1,42,43] For inorganic thin films derived by sol−gel chemistry cracks can form at multiple processing stages. We designed a sol−gel dip-coating method optimized to address these challenges at the three most important processing stages: the initial film drying, the preannealing step, and the annealing (heat treatment) process. The major steps of our process for fabricating highly reproducible, large-area, crack-free, single and multilayer structures of silica and titania, as well as stacks of alternating layers of these two compounds, are schematically shown in Figure 1.

During the drainage process, which starts immediately after the film withdrawal in the dip-coating process, inhomogeneous solvent evaporation within the film creates a pressure gradient.[27,44] The gradient causes a differential shrinkage of the thin-film network, whereby the exterior of the network shrinks faster than the interior. This leads to the build-up of tensile stresses that can fracture the thin film upon ongoing solvent evaporation.[1] We found this problem can be overcome by designing the dip-coating process such that the freshly deposited film is withdrawn into an environment of high solution−vapor pressure. This is achieved simply by using a tall vial that was only half-filled with the deposition solution (Figure 1a). The deposited film is subsequently subjected to a drying step in a flowing hot-air stream generated by a heat gun (Figure 1b), resulting in a rapid and homogeneous solvent evaporation. We found the combination of these two steps counteracts the differential shrinkage within the deposited layer and results in formation of crack-free films (Figure 2a, b). In addition, the heat-gun treatment greatly reduced the occurrence of edge effects. Edge effects in deposited thin films are a known phenomenon especially associated with dip-coating processes, and are caused by substrate vibrations and inhomogeneous solvent evaporation in the center and at the edges of deposited films during the withdrawal process.[45]

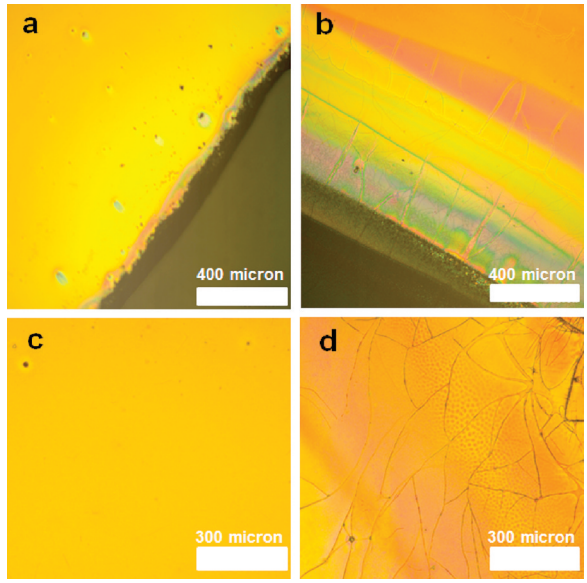

Figure 2. Optical micrographs of 12 alternating silica/titania thin-film layers deposited onto a silicon (100) wafer. Top: Samples fabricated (a) including and (b) omitting the dry-blowing step in the deposition cycle (Figure 1). Bottom: Samples fabricated (c) including and (d) omitting the shock-cooling step in the deposition cycle (Figure 1).

Heat-treatment of the deposited films is the final stage of the fabrication process. During heat-treatment residual solvent and other organic components of the precursor solution are pyrolytically removed and the loosely formed oxide network is further densified. In the case of titania films, heat-treatment also leads to partial crystallization of the initially amorphous network. However, these reactions during heat-treatment also lead to further film shrinkage, accompanied by an increase in tensile stresses, potentially causing crack formation. On the other hand, it is known that rapid heating rates increase the viscoelasticity of the initially forming amorphous oxide network.[28,42,43] This network relaxation counteracts the tensile stress formation and suppresses crack formation. We found placing the deposited and hot-air treated films into a preheated oven at 350−500 °C for 1 min gave the best results (Figure 1c).

Similar to the heating process the cool-down stage must be optimized to create high-quality films. While this stage of the heat-treatment is often neglected, we found it to be of particular

dx.doi.org/10.1021/cm202019b | Chem. Mater. 2011, 23, 5177−5184

importance for fabricating crack-free thin-film stacks composed of alternating layers of silica and titania. Several factors are responsible for the formation of cracks during the cool-down process. One source is the difference in expansion coefficients between the alternating deposited layers as well as between the substrate and the deposited film. Another source of cracking is reorganization of the thin film metal oxide network. This reorganization is caused by phase transitions of the amorphous or amorphous/polycrystalline network upon cooling, leading to build-up of stresses that can fracture the film network.[28] We studied the cool-down process in detail and found that—similar to the heating stage—rapid cooling rates are beneficial in the prevention of crack formation (Figure 2c, d). Although perhaps counterintuitive, we found the best results were obtained by shock-cooling the film samples to room temperature immediately following the 1 min heating period. Shock-cooling was achieved by placing the hot samples onto a Pyrex glass substrate at room temperature or immersing them into a water/isopropanol mixture (Figure 1d). While the exact mechanism is still under investigation, we propose rapid cooling minimizes the occurrence of interfacial stresses (due the difference in thermal expansion coefficients of alternating layers). In addition, temperature quenching freezes high-temperature amorphous/polycrystalline phases,[46] maintaining high viscoelasticity of the oxide network at room temperature.

Deposition of Bragg Stacks on Various Substrates. To demonstrate the effectiveness of our sol–gel process in fabricating high-quality multilayer structures, we fabricated a Bragg stack of seven alternating silica/titania layers (14 layers in total). The Bragg stack was fabricated on a silicon wafer (100) substrate using the thin film deposition cycle described above (Figure 3a). The deposition parameters were tuned to yield

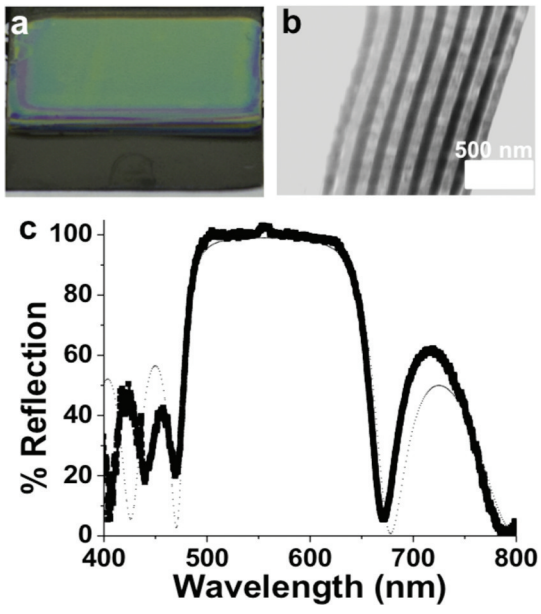

Figure 3. (a) Photograph and (b) cross-sectional SEM image of a thin-film Bragg stack consisting of 14 alternating layers of silica (88 ± 2 nm; dark layers) and titania (75 ± 2 nm; bright layers) deposited onto a silicon (100) wafer. (c) Corresponding optical reflection spectrum (solid line) and simulated spectrum (dotted line).

layer thicknesses of 88 ± 2 nm (silica) and 75 ± 2 nm (titania) after calcination at 500 °C. At this temperature, the titania network predominantly forms an anatase polycrystalline phase,[47,48] as was confirmed by XRD measurements. The structural features of the Bragg stack were examined by optical and electron microscopy. Optical imaging revealed a smooth surface and absence of even microcracks, and cross-sectional SEM imaging verified the high degree of thickness uniformity throughout the multilayer stack (Figure 3b). It should be emphasized that this deposition process is capable of producing uniform multilayer stacks over large areas. For example, Figure S2 (Supporting Information) shows a Bragg stack of six alternating silica/titania layers (12 layers in total) deposited over an area of 20 cm^2.

The excellent structural uniformity is also reflected in the optical properties of the Bragg stacks, acting as 1D photonic bandgap materials. As expected for a high-quality 1D photonic bandgap structure, our 14-layer sample displayed an optical reflection peak with a broad wavelength range of 100% reflectivity (Figures 3c). In general, we found six to seven alternating double layers are necessary to achieve a bandgap with 100% reflectivity in the visible range of the electromagnetic spectrum. For the 88/75 nm silica/titania Bragg stack we measured a broad reflection band centered at a wavelength position of 575 nm and a width of 6200 cm^{-1} (around 200 nm) at normal incidence. The reproducibility of our deposition process was confirmed by fabricating three samples at different times but under the same experimental conditions (i.e., precursor solution composition, dip-coating parameters, drying and heat treatments). The optical reflection properties of the three samples are given in Figure S3 (Supporting Information) and show near-identical optical features in terms of reflection band position, width and shape (including side bands). Importantly, the measured reflection data are in excellent agreement with the calculated reflection spectrum (dotted line in Figure 3c). For the calculation, we used the film thickness (SEM imaging, ellipsometry), the number of layers, and the refractive index of each layer (determined by ellipsometry) as input parameters.

It should be emphasized that our sol–gel deposition method can be applied to a number of different substrates. For example, to produce optical filters we used quartz or borosilicate glass substrates (Figure 4a). Optical characterization reveals almost identical reflection features, confirming the high optical quality of the samples regardless of the substrate (Figure 4c). Note that borosilicate substrates, for example, would be incompatible with often-used high-temperature (900–1000 °C) firing methods. The versatility of our sol–gel method is further demonstrated by depositing the same Bragg stacks onto curved quartz and glass substrates. As shown in image b and panel d in Figure 4, samples deposited onto curved substrates show excellent optical properties and are interesting candidates for parabolic high-power laser mirrors and solar radiation collectors. For all samples, the calculated reflection spectra are also included (dotted lines), demonstrating again the good optical performance of the Bragg stacks regardless of the substrates used.

Tuning the Position and Width of the Photonic Bandgap. Because Bragg stacks behave as 1D photonic bandgap materials, the width and the position of the optical reflection band (bandgap) can be tuned by adjusting the refractive index difference and the thickness, respectively, of the alternating layers.[49,50] The ability to tune the bandgap position is demonstrated in Figure 5. Varying the lattice constant (one silica/titania double-layer) from 148 ± 2 to 168 ± 2 nm (in 5 nm steps) shifts the reflection band throughout the entire visible range. The lattice constant variation was achieved by

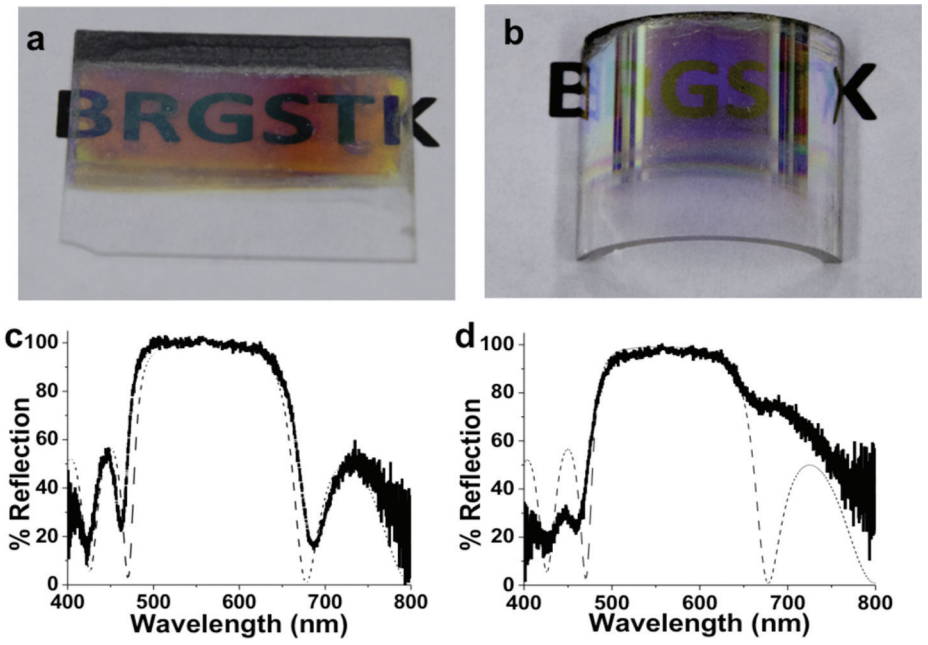

Figure 4. (a, b) Photographs of thin-film Bragg stacks consisting of 12 alternating layers of silica (88 ± 2 nm; dark layers) and titania (75 ± 2 nm; bright layers) deposited onto (a) a planar borosilicate glass substrate and (b) a curved quartz-glass substrate. (c, d) Corresponding optical reflection spectra (solid lines) of the stacks on (c) a planar borosilicate glass substrate and (d) a curved quartz-glass substrate. Simulated spectra are given as dotted lines.

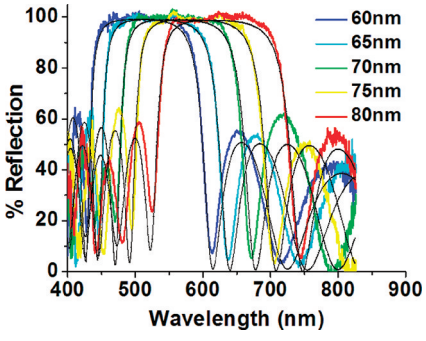

Figure 5. Optical reflection spectra of Bragg stacks of 12 alternating silica/titania layers. The silica layer thickness was held constant at 88 ± 2 nm, whereas the titania layer thickness was varied between 60 ± 2 and 80 ± 2 nm, as indicated in the figure. The simulated spectra are given as dotted lines.

adjusting the titania layer thickness for each sample while keeping the silica layer thickness constant at 88 ± 2 nm. Experimentally, this was done simply by diluting the titania precursor solution with additional ethanol while keeping the silica precursor concentration and the dip-coating parameters constant. The degree of dissolution was adjusted in response to ellipsometry measurements and SEM cross-sectional imaging (see also Figure S1 in Supporting Information). Additionally, simulations were used to verify the experimentally obtained reflection band positions and other optical features. Again, as shown by the dotted spectra in Figure 5, excellent agreement was achieved.

The width of the photonic bandgap can be tuned by modifying the difference in the refractive indices of the alternating layers; in general, the smaller the difference the narrower the gap. Although the refractive indices of titania and silica obtained by our sol–gel method are fixed (2.34 ± 0.02 for titania and 1.48 ± 0.02 for silica), we found that tuning the difference is possible by fabricating composite layers. For example, diluting the titania layers with a given amount of silica, lowers the effective refractive index from 2.34 to a value given by the silica volume fraction (dilution factor). Building a Bragg stack with silica-diluted titania layers while leaving the silica layers unchanged thus reduces the refractive index difference and should narrow the bandgap.

Diluting the titania layers was achieved by first adding a block copolymer surfactant (Pluronic P123) to the titania precursor solution.[6,40] After film dip-coating the organic surfactant is thermally removed during the heat-treatment, leaving behind a disordered nanoporous titania framework. A TEM image of a titania film deposited from a precursor solution containing 0.5 g of P123 is shown in Figure 6a and reveals the nanoscale

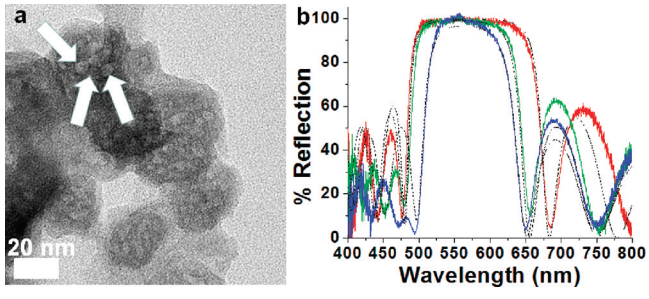

Figure 6. (a) TEM image of a nanoporous titania thin-film sample. Some of the pores are indicated by arrows. (b) Optical reflection spectra of three 14-layer silica/titania Bragg stacks with differing refractive indices of the titania layer deposited onto a silicon (100) substrate. The titania layer refractive indices are 2.34 ± 0.02 (red spectrum), 2.1 ± 0.1 (green spectrum), and 1.8 ± 0.1 (blue spectrum). Simulated spectra are given as dotted lines.

porosity. During the following dip-coating step of a layer of silica, also the porous titania framework is infiltrated with the silica precursor solution. Because the degree of silica dilution is

dx.doi.org/10.1021/cm202019b | *Chem. Mater.* 2011, 23, 5177–5184

given by the degree of porosity of the titania layer, it can readily be tuned by the amount of P123 mixed into the titania precursor solution. For example, addition of 0.3 and 0.5 g of P123 resulted in silica–titania composite layers with refractive indices of 2.1 ± 0.1 and 1.8 ± 0.1, respectively. These values were obtained by fitting the measured optical reflectance data to simulated spectra of Bragg stacks with known lattice constants and layer thicknesses (measured by SEM imaging). Figure 6b illustrates the tunability of the reflection bandwidth (photonic bandgap) for three Bragg stacks with decreasing refractive index differences between the alternating layers.

Design of Optical Microcavities and Asymmetric Stacks. The simplicity and flexibility of our sol–gel dip-coating route readily allows to create multilayer structures with built-in asymmetry. For example, Figure 7a shows a cross-section SEM image of a multilayer stack with a central "defect layer", breaking the symmetry of the periodic stack. The overall structure consists of a central silica layer with a thickness of 176 ± 2 nm sandwiched between two Bragg stacks each composed of four silica/titania double layers with a lattice constant of 158 ± 2 nm and individual layer thicknesses of 88 ± 2 nm (silica) and 70 ± 2 nm (titania). The 176 nm silica layer was fabricated simply by depositing two successive 88 nm silica layers. The optical reflection spectrum of the final structure is given in Figure 7b and displays the typical characteristic of a Fabry–Perot microcavity, namely, a narrow high-transmittance region (localized optical mode) within the optical reflection band (photonic bandgap). The transmission peak maximum (70% transmittance) is located at a wavelength position of 568 nm and has a full-width-half-maxim value, $\Delta\lambda$, of 5 nm for normal incidence of unpolarized light. This yields a quality factor, $Q = \Delta\lambda/\lambda$, of 112 for the microcavity. Similar to tuning the optical properties of Bragg stacks, the wavelength position of the localized cavity mode can be tuned by modifying the structural features (lattice constant and layer thicknesses) of the Fabry–Perot microcavity design.

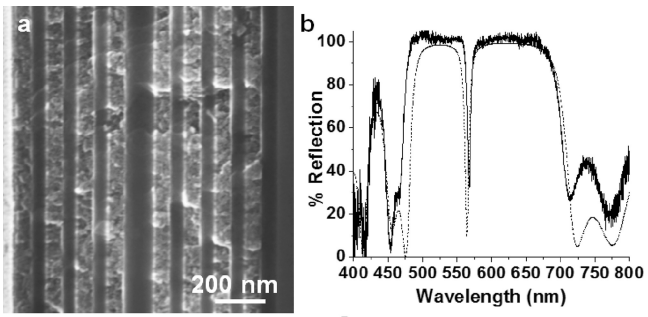

Figure 7. (a) Cross-sectional SEM image and (b) optical reflection spectrum of a Fabry–Perot microcavity structure deposited onto a silicon (100) substrate. The microcavity is composed of a central silica defect layer with a thickness of 176 ± 2 nm sandwiched between two 8-layer silica/titania Bragg stacks with silica and titania thicknesses of 88 ± 2 and 70 ± 2 nm, respectively. The optical cavity mode occurs at a wavelength position of 568 nm. The simulated spectrum is given as dotted line.

Another possibility of producing interesting optical features is to gradually induce asymmetry into a multilayer stack. An example is shown in Figure 8a. In this 25-layer structure of alternating silica and titania films the silica layer thickness was held constant at 44 ± 2 nm, while the thickness of the titania layers is successively increased from 68 ± 2 nm (left edge) to 88 ± 2 nm (center) in 5 nm steps, and then successively decreased again to 68 ± 2 nm (right edge). The resulting optical reflection spectrum (Figure 8b) shows interesting features with the appearance of four narrow transmission modes between 400 and 550 nm, which are in excellent agreement with the calculated spectra. This agreement between experiment and theory for such an elaborate asymmetric multilayer stack not only shows the precise control over single-layer thickness deposition, but also confirms the reproducibility of our simple sol–gel deposition approach over tens of consecutive layers. The presence of these narrow optical modes in our microcavity structures and asymmetric Bragg stacks should make these samples interesting candidates for light amplification applications and we are currently investigating possibilities to incorporate light sources into our samples.

■ CONCLUSIONS

We have developed a sol–gel chemistry-based dip-coating method with all the desirable attributes of solution processing—simple, fast, inexpensive, and versatile—and yet produces high-quality thin-film single and multilayer structures, rivaling

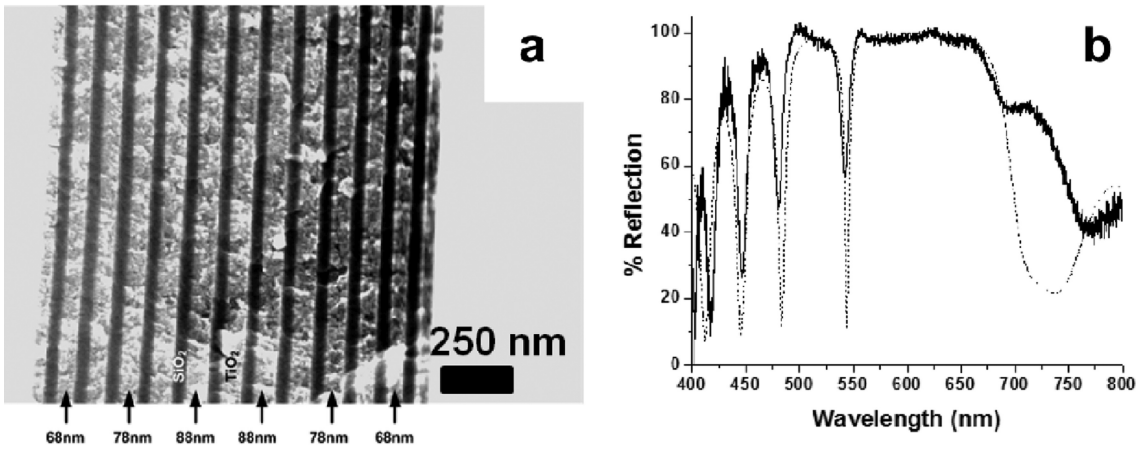

Figure 8. (a) Cross-sectional SEM image and (b) optical reflection spectrum of an asymmetric 25-layer silica/titania Bragg stack deposited onto a silicon (100) substrate. The silica layer thickness was held constant at 44 ± 2 nm, whereas the titania layer thickness was varied in 5 nm steps from 68 ± 2 nm to 88 ± 2 nm and back to 68 ± 2 nm. The simulated spectrum is given as dotted line.

dx.doi.org/10.1021/cm202019b | Chem. Mater. 2011, 23, 5177–5184

those fabricated by expensive physical and chemical deposition methods. We discussed causes of typical limitations of sol−gel thin-film processing such as crack formation and occurrence of structural inhomogeneities in multilayer stacks, and introduced strategies to overcome these limitations. We demonstrated that controlled and homogeneous solvent evaporation of the as-deposited films as well as rapid heating and cooling rates are keys in preventing crack formation. The latter proved particularly important for the fabrication of crack-free silica/titania multilayer stacks with precise and reproducible thicknesses of up to 25 alternating layers. Moreover, we showed that such multilayer stacks can be deposited on a variety of substrates over large areas with planar and even curved geometries without loss of structural features.

We used our sol−gel dip-coating process to fabricate high-quality optical components, including Bragg-type reflectors and filters, Fabry−Perot microcavities, and asymmetric stacks. These photonic bandgap-based structures displayed tunable optical properties with wide reflection bands and well-defined localized cavity modes. The wavelength position of the photonic bandgap and the cavity mode can readily be tuned throughout the entire visible range by controlling the layer thickness during the dip-coating process. Tuning the width of the optical reflection band was demonstrated by fabricating titania-silica nanostructured composite layers with different titania-to-silica ratios. Experimentally obtained reflection spectra were also compared to results from simulations using the transfer-matrix method. Very good agreement was found between the measured and calculated results, confirming again the high precision and reproducibility of the fabrication process. To conclude, the versatility of sol−gel chemistry combined with our inexpensive and rapid thin-film processing route (a 20-layer silica/titania stack can be fabricated in less than 2 h) makes our method an attractive alternative to conventional physical/chemical deposition and sputtering techniques. The fabricated multilayer photonic bandgap structures possess excellent structural and optical properties and should be interesting candidates for use in optical and electronic applications.

■ ASSOCIATED CONTENT

Supporting Information

Photograph of a large-area (5 × 4 cm) multilayer stack sample, reflection spectra showing sample-to-sample reproducibility, and graphs depicting the thickness of deposited films vs degree of dilution of the precursor solution with ethanol. This material is available free of charge via the Internet at http://pubs.acs.org.

■ AUTHOR INFORMATION

Corresponding Author

*E-mail: bartl@chem.utah.edu.

■ ACKNOWLEDGMENTS

We thank Jessica Pauley, Todd Anderson, and Karine Chesnel for valuable contributions. We further thank Brian van Devener (Surface Analysis and Nanoimaging Lab, University of Utah), the Porter Group (University of Utah) for their help in ellipsometry measurements, and Jeffrey Farrer (BYU Microscopy lab) for help with TEM studies. This work was supported in part by the National Science Foundation under Award DMR-1005382, the U.S. Department of Energy under Contract DE-EE0002768, and by start-up funds from the University of Utah.

■ REFERENCES

(1) Brinker, C. J.; Scherer, G. W. *Sol−Gel Science*; Academic Press: San Diego, CA, 1990.
(2) Livage, J.; Henry, M.; Sanchez, C. *Prog. Solid State Chem.* **1988**, *18*, 259.
(3) Dimitriev, Y.; Ivanova, Y.; Iordanova, R. *J. UCTM* **2008**, *43*, 181.
(4) Innocenzi, P.; Zub, Y. L.; Kessler, V. G., Eds. *Sol−Gel Methods for Materials Processing*; Springer: Dordrecht, The Netherlands, 2008.
(5) Sanchez, C.; Boissière, C.; Grosso, D.; Laberty, C.; Nicole, L. *Chem. Mater.* **2008**, *20*, 682.
(6) Bartl, M. H.; Boettcher, S. W.; Frindell, K. L.; Stucky, G. D. *Acc. Chem. Res.* **2005**, *38*, 263.
(7) Schubert, U.; Huesing, N.; Lorenz, A. *Chem. Mater.* **1995**, *7*, 2010.
(8) Chujo, Y. *Curr. Opin. Solid State Mater. Sci* **1996**, *1*, 806.
(9) Yang, P.; Deng, T.; Zhao, D.; Feng, P.; Pine, D.; Chmelka, B. F.; Whitesides, G. M.; Stucky, G. D. *Science* **1998**, *282*, 2244.
(10) Angelomé, P. C.; Fuertes, M. C.; Soler-Illia, G. J. A. A. *Adv. Mater.* **2006**, *18*, 2397.
(11) Stucky, G. D.; Bartl, M. H. In *Thin Film Metal-Oxides: Fundamentals and Applications in Electronics and Energy*; Ramanathan, S., Ed.; Springer: New York: 2010, p 255.
(12) Yao, H.-B.; Fang, H.-Y.; Wang, X.-H.; Yu, S.-H. *Chem. Soc. Rev.* **2011**, *40*, 3764.
(13) Kobler, J.; Lotsch, B. V.; Ozin, G. A.; Bein, T. *ACS Nano* **2009**, *3*, 1669.
(14) Hidalgo, N.; Calvo, M. E.; Colodrero, S.; Miguez, H. *IEEE Sens. J.* **2010**, *10*, 1206.
(15) Scott, B. J.; Wirnsberger, G.; Stucky, G. D. *Chem. Mater.* **2001**, *13*, 3140.
(16) Maex, K.; Baklanov, M.; Shamiryan, D.; Iacopi, F.; Brongersma, S.; Yanovitskaya, Z. *J. Appl. Phys.* **2003**, *93*, 8793.
(17) Volksen, W.; Miller, R. D.; Dubois, G. *Chem. Rev.* **2009**, *110*, 56.
(18) Subban, C. V.; Zhou, Q.; Hu, A.; Moylan, T. E.; Wagner, F. T.; DiSalvo, F. J. *J. Am. Chem. Soc.* **2010**, *132*, 17531.
(19) Knez, M.; Nielsch, K.; Niinistö, L. *Adv. Mater.* **2007**, *19*, 3425.
(20) Pore, V.; Ritala, M.; Leskelä, M.; Areva, S.; Järn, M.; Järnström, J. *J. Mater. Chem.* **2007**, *17*, 1361.
(21) Ashfold, M. N. R.; May, P. W.; Rego, C. A.; Everitt, N. M. *Chem. Soc. Rev.* **1994**, *23*, 21.
(22) Bhakta, R.; Thomas, M.; Hipler, F.; Bettinger, H. F.; Müller, J.; Ehrhart, P.; Devi, A. *J. Mater. Chem.* **2004**, *14*, 3231.
(23) Kunkel, R.; Poelsema, B.; Verheij, L. K.; Comsa, G. *Phys. Rev. Lett.* **1990**, *65*, 733.
(24) Safi, I. *Surf. Coat. Technol.* **2000**, *127*, 203.
(25) Kelly, P. J.; Arnell, R. D. *Vacuum* **2000**, *56*, 159.
(26) Wang, C. W.; Chen, S. F.; Chen, G. T. *J. Appl. Phys.* **2002**, *91*, 9198.
(27) Faustini, M.; Louis, B.; Albouy, P. A.; Kuemmel, M.; Grosso, D. *J. Phys. Chem. C* **2010**, *114*, 7637.
(28) Kozuka, H.; Takenaka, S.; Tokita, H.; Hirano, T.; Higashi, Y.; Hamatani, T. *J. Sol−Gel Sci. Technol.* **2003**, *26*, 681.
(29) O'Regan, B.; Grätzel, M. *Nature* **1991**, *353*, 737.
(30) Ni, M.; Leung, M. K. H.; Leung, D. Y. C.; Sumathy, K. *Renewable Sustainable Energy Rev.* **2007**, *11*, 401.
(31) Khan, S. U. M.; Al-Shahry, M.; Ingler, W. B. *Science* **2002**, *297*, 2243.
(32) Yoldas, B. E.; O'Keeffe, T. W. *Appl. Opt.* **1979**, *18*, 3133.
(33) Hinczewski, D. S.; Hinczewski, M.; Tepehan, F. Z.; Tepehan, G. G. *Sol. Energy Mater. Sol. Cells* **2005**, *87*, 181.
(34) Li, Y.; Fortes, L. M.; Chiappini, A.; Ferrari, M.; Almeida, R. M. *J. Phys. D: Appl. Phys.* **2009**, *42*, 205104.
(35) Bellessa, J.; Rabaste, S.; Plenet, J. C.; Dumas, J.; Mugnier, J.; Marty, O. *Appl. Phys. Lett.* **2001**, *79*, 2142.
(36) Jasieniak, J.; Sada, C.; Chiasera, A.; Ferrari, M.; Martucci, A.; Mulvaney, P. *Adv. Funct. Mater.* **2008**, *18*, 3772.

(37) Rabaste, S.; Bellessa, J.; Brioude, A.; Bovier, C.; Plenet, J. C.; Brenier, R.; Marty, O.; Mugnier, J.; Dumas, J. *Thin Solid Films* **2002**, *416*, 242.
(38) Jiang, K.; Zakutayev, A.; Stowers, J.; Anderson, M. D.; Tate, J.; McIntyre, D. H.; Johnson, D. C.; Keszler, D. A. *Solid State Sci.* **2009**, *11*, 1692.
(39) Saleh, E. A. B.; Malvin, T. C. *Fundamentals of Photonics*; John Wiley & Sons: New York, 1991.
(40) Bartl, M. H.; Puls, S. P.; Tang, J.; Lichtenegger, H. C.; Stucky, G. D. *Angew. Chem., Int. Ed.* **2004**, *43*, 3037.
(41) Larouche, S.; Martinu, L. *Appl. Opt.* **2008**, *47*, C219.
(42) Bockmeyer, M.; Löbmann, P. *Chem. Mater.* **2006**, *18*, 4478.
(43) Bockmeyer, M.; Löbmann, P. *Thin Solid Films* **2007**, *515*, 5212.
(44) Scriven, L. E. In *Better Ceramics Through Chemistry III*; Brinker, C. J., Clark, D. E., Ulrich, D. R., Eds.; Mateial Research Society: Pittsburgh, PA, 1988, p 717.
(45) Schüler, A.; Dutta, D.; de Chambrier, E.; Roecker, C.; De Temmerman, G.; Oelhafen, P.; Scartezzini, J.-L. *Sol. Energy Mater. Sol. Cells* **2006**, *90*, 2894.
(46) MacLeod, A. H. *Thin-Film Optical Filters*; Institute of Physics Publishing: Bristol, U.K., 2001.
(47) Kuznetsova, I. N.; Blaskov, V.; Znaidi, L. *Mater. Sci. Eng., B* **2007**, *137*, 31.
(48) Rath, H.; Dash, P.; Som, T.; Satyam, P. V.; Singh, U. P.; Kulriya, P. K.; Kanjilal, D.; Avasthi, D. K.; Mishra, N. C. *J. Appl. Phys.* **2009**, *105*, 074311.
(49) Fink, Y.; Winn, J. N.; Fan, S.; Chen, C.; Michel, J.; Joannopoulos, J. D.; Thomas, E. L. *Science* **1998**, *282*, 1679.
(50) Lee, H.-Y.; Yao, T. *J. Appl. Phys.* **2003**, *93*, 819.